Available online at www.sciencedirect.com
SCIENCE DIRECT®
Surface Science 591 (2005) L286–L291
SURFACE SCIENCE
www.elsevier.com/locate/susc

Surface Science Letters

Evidence of surface reconstruction during 'bioinspired' inorganic nucleation at an organic template

S. Kewalramani [a,*], G. Evmenenko [a], C.-J. Yu [b], K. Kim [a], J. Kmetko [a,1], P. Dutta [a]

[a] *Department of Physics and Astronomy, Northwestern University, Evanston, IL 60208-3112, USA*
[b] *Pohang Accelerator Laboratory, Pohang, Kyungbuk 790-330, South Korea*

Received 23 March 2005; accepted for publication 20 June 2005
Available online 2 August 2005

Abstract

X-ray diffraction studies performed during the nucleation of hydrocerussite ($PbCO_3 \cdot Pb(OH)_2$) from a supersaturated aqueous solution, at a floating fatty acid monolayer template, reveal ($\sqrt{7} \times \sqrt{7}$)-*R*19.1° reconstruction at the (0 0 1) surface of hydrocerussite. Reordering of surface atoms into epitaxial superstructures is thought to require extremely clean surfaces (cleaned electrochemically or under UHV). At this organic–inorganic interface, the organic monolayer relaxes to form an epitaxial match with the reconstructed lattice just below it. We speculate that this lattice match, along with the ion-specific interactions of the monolayer, provide the clean nucleation environment.

Keywords: X-ray diffraction; Nucleation; Surface relaxation and reconstruction; Epitaxy; Soft–hard interface; Biomineralization

The process of biomineralization [1] is characterized by molecular control of crystallographic structure, orientation and particle size at the organic–inorganic interface. Organic-template-directed inorganic crystal nucleation mimics this biological process. Monomolecular layers of insoluble surfactants, floating at the surfaces of supersaturated aqueous solutions, are widely used for studying nucleation and growth of minerals at organized organic surfaces [2]. These monolayers, because of their ordered two-dimensional hydrophilic head groups, are thought to form templates for the inorganic lattice. Such Langmuir monolayers form excellent systems for studying organic–inorganic interface phenomena, because of the

* Corresponding author. Tel.: +1 312 404 6205; fax: +1 847 491 9982.
E-mail addresses: s-kewalramani@northwestern.edu (S. Kewalramani), pdutta@northwestern.edu (P. Dutta).
[1] Present Address: Department of Physics, Cornell University, Ithaca, NY 14853, USA.

0039-6028/$ - see front matter
doi:10.1016/j.susc.2005.06.086

ease of experimental control and accessibility to structural probes such as X-ray diffraction [3]. Oriented crystal growth of $CaCO_3$ [4], PbS and CdS [5], $BaSO_4$ [6], BaF_2 [7], SrF_2 [8], etc. from supersaturated solutions under Langmuir monolayers has been reported. We have grown hydrocerussite (lead dihydroxide carbonate) in the same way, but also performed in situ grazing incidence X-ray diffraction scans during the nucleation process.

Monolayers of heneicosanoic acid, $C_{20}H_{41}$-COOH, were spread over subphases prepared by mixing equal volumes of aqueous solutions of lead chloride (4×10^{-5} and 8×10^{-5} M) and sodium bicarbonate (8×10^{-5} and 16×10^{-5} M). The monolayers were then compressed by a mechanical barrier until the surface pressure rose slightly above 0 dynes/cm. This ensures that the monolayer is all in a single phase rather than a coexistence of a gas phase and a condensed phase. The pH of the subphase was left unadjusted and was measured to be 5.7 ($\pm$0.3) at the time of sample preparation. The temperature was maintained at 20 °C during all measurements. A beam of synchrotron X-rays with $\lambda = 1.5498$ Å was incident upon the water surface in the grazing incidence diffraction geometry. Vertical and horizontal soller slits in front of the detector defined a horizontal resolution $K_{xy} \sim 0.01$ Å^{-1} full width at half maximum (FWHM) and a vertical resolution $K_z \sim 0.05$ Å^{-1} FWHM. Other details of the experimental setup can be found in Ref. [9]. As Langmuir monolayers are powders in the horizontal plane, the in-plane momentum transfer vector K_{xy} cannot be decomposed into x- and y-components. However, the important vertical component K_z can be measured separately.

Before commencement of inorganic nucleation at the interface, three in-plane peaks at $K_{xy} =$ 1.484, 1.520 and 1.635 Å^{-1} are observed. These peaks are due to the organic monolayer; this structure is known to occur in carboxylic acid monolayers on lead ion solutions [10] above a threshold concentration. As also previously reported, an ordered inorganic *monolayer* forms under the organic film; we observed the strongest of the diffraction peaks (appearing in the region 0.3–0.6 Å^{-1}) due to this superlattice. (These data are not shown here, but see Ref. [10].)

The schematic drawing (Fig. 1) summarizes the nucleation process. As a thicker inorganic layer grows at the water surface, the organic monolayer assumes a different structure. Two first-order diffraction peaks are now seen, one in-plane (0 1) and one out of plane ((1 0) + (1 −1)) (Fig. 2). These peaks can be identified as due to the organic film because the diffraction peaks have a width in the z-direction (Bragg rod widths) consistent with the thickness of heneicosanoic acid monolayer (~30 Å). The diffraction peaks indicate that the organic head groups arrange in a symmetrically

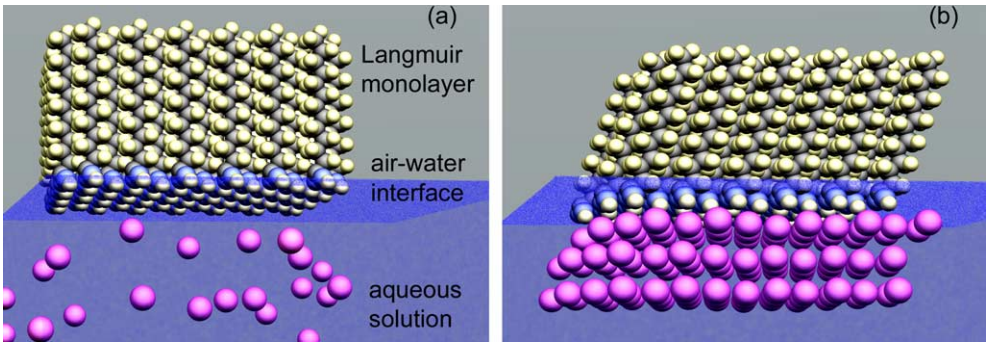

Fig. 1. Schematic diagram of the nucleation process being studied: (a) before inorganic nucleation at the interface, the floating organic molecules are oriented along the interface normal; (b) during inorganic nucleation, the organic molecules rearrange and also tilt away from the surface normal.

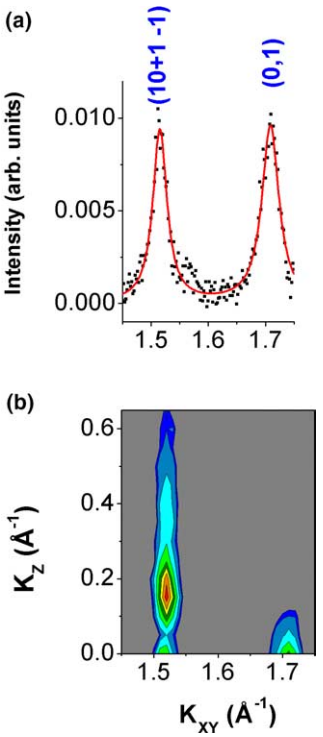

Fig. 2. Langmuir monolayer structure, during hydrocerussite nucleation: (a) in-plane scan at $K_{xy} = 0$, showing the two first-order diffraction peaks; (b) intensity contours in the K_z/K_{xy} plane for these peaks, showing that the first peak is above the monolayer plane while the second is in the plane.

distorted hexagonal pattern with the molecule tails tilted at an angle of 7.2° in the nearest neighbor direction. The primitive cell of the monolayer has lattice parameters $|\underset{\sim}{a}_m| = 4.99$ Å, $|\underset{\sim}{b}_m| = 4.45$ Å, $\gamma_m = 124.1°$, and an area, $A_m = 18.39$ Å^2/molecule. These conclusions are confirmed by the observation of three second-order diffraction peaks (20), (2−1) and ((−12) + (11)); these are not shown here. The average lateral size of the organic domains estimated from peak widths is ~200 Å.

We also see diffraction peaks arising from the nucleating inorganic material. These peaks can be distinguished unambiguously from organic peaks, as they are much sharper in the horizontal plane. The diffraction peaks arise from two distinct structures. The six peaks due to the known bulk structure of hydrocerussite [11] have resolution limited widths in the horizontal direction corresponding to lateral crystallite size >550 Å.

Gaussian fits to the out of plane scans indicate a inorganic layer thickness >150 Å, which is higher than the e-folding penetration depth (~100 Å) of the X-rays. Thus, the X-ray penetration depth limits the estimation of the thickness of this bulk layer. Two of these peaks are shown in Fig. 3(a). The positions of these peaks show that the bulk crystals are oriented with their (0 0 1) crystal planes parallel to the interface. The unit cell parameters for the hexagonal face of hydrocerussite (the (0 0 1) plane) are $|\underset{\sim}{a}_b| = 5.24$ Å, $\gamma_b = 120°$, and unit cell area, $A_b = 23.78$ Å^2.

The remaining peaks are much weaker than the bulk hydrocerussite peaks. They are sharp in the horizontal plane (lateral domain size (~400 Å) but broad along the Bragg rods, indicating that they are due to a thin (~40 Å) layer, presumably at the surface. Two of these peaks (both at the same K_{xy}) are shown in Fig. 3(b), and all observed peaks are shown in Fig. 3(c). The horizontal components of the momentum transfer vectors from all the weaker reflections can be indexed in fractions of the corresponding components of the hydrocerussite reciprocal lattice vectors (Fig. 3(c)). The indexing is consistent with a $(\sqrt{7} \times \sqrt{7})$-$R19.1°$ supercell, i.e., a hexagonal structure with an area 7 times that of the (0 0 1) oriented plane of the bulk nucleate. The peak positions also show that the surface hexagonal lattice is oriented with its c-axis normal to the liquid plane. The lateral lattice parameters for this superlattice are, $|\underset{\sim}{a}_s| = 13.87$ Å, $\gamma_s = 120°$, and area $A_s = 166.6$ Å^2.

The relationship between the (0 0 1) plane of the bulk crystal and the reconstructed structure is shown in real space in Fig. 4(a). The surface layer basis vectors $(\underset{\sim}{a}_s, \underset{\sim}{b}_s)$ are related to the bulk lateral basis $(\underset{\sim}{a}_b, \underset{\sim}{b}_b)$ by $\underset{\sim}{a}_s = 2\underset{\sim}{a}_b - \underset{\sim}{b}_b$, $\underset{\sim}{b}_s = \underset{\sim}{a}_b + 3\underset{\sim}{b}_b$. These relationships are accurate to 0.1%.

It can be seen from the contour plots in Fig. 3(c), and more clearly in the rod scans shown in Fig. 5(b), that the fractional-index reflections from the surface superlattice have distinct features in the z-direction; they are not from a two-dimensional array of points. The in-plane peaks are observed only for reciprocal lattice vectors with horizontal-plane indices for which $h - k = 3n/7$,

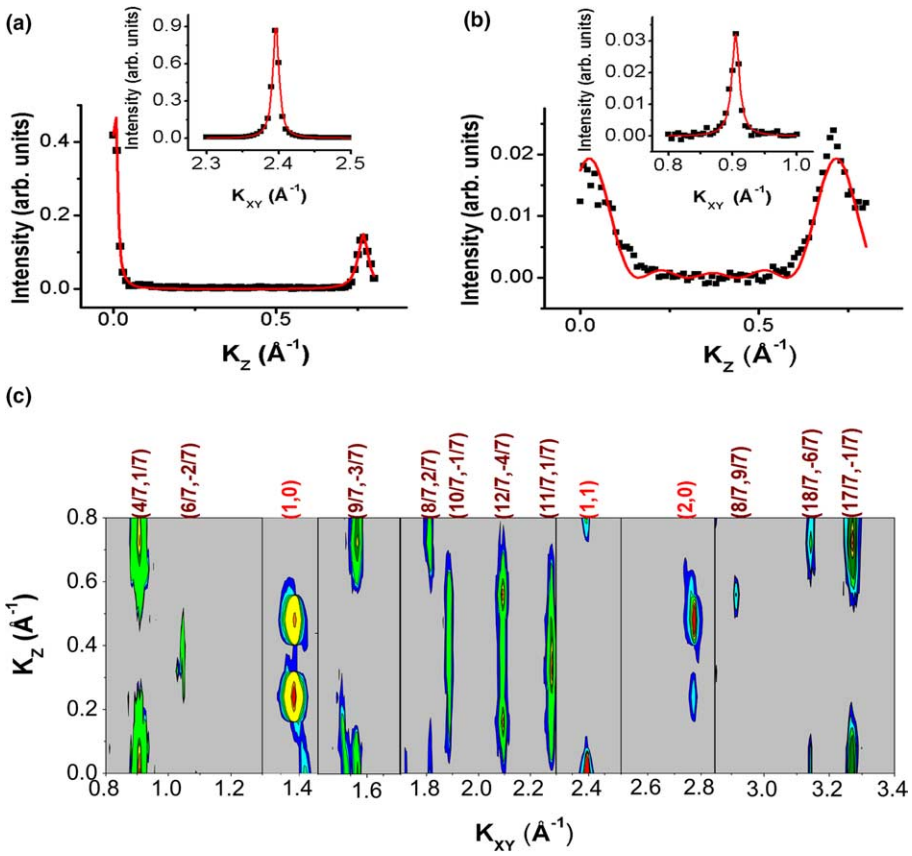

Fig. 3. Comparison between diffraction peaks from bulk and surface inorganic lattices: (a) vertical scan through the hydrocerussite (1 1 0) and (1 1 3) peaks. Inset shows a horizontal scan through the (1 1 0) peak; (b) vertical scans through the (11/7, 1/7) peak due to surface layers. Inset shows the (11/7, 1/7) peak at its Bragg position. The intensity of the hydrocerussite peaks is an order of magnitude higher than those from the surface structure. Further, the intensity falls off sharply as a function of K_z in (a), implying that the peaks are due to a thicker film (>100 Å) compared to the Bragg rod in (b), which indicates a thickness of ~40 Å; (c) intensity contours constructed from diffraction data during hydrocerussite nucleation from a supersaturated aqueous solution subphase. The six peaks labeled with integer indexes correspond to bulk hydrocerussite. The fractional order peaks (all of which are very broad in the z-direction) are from a $\sqrt{7} \times \sqrt{7}$ interfacial superlattice ~40 Å thick.

indicating that the superlattice structure along the c-axis is a hexagonal close-packed structure with multiple layers arranged in some combination of A, B and C type layers.

Since our peak positions are perfectly reproducible but the peak intensities vary somewhat from scan to scan, we cannot follow the usual methods of three-dimensional crystallography such as Patterson function analysis or the calculation of structure reliability index. Instead, we have fitted the data assuming that all the layers are the same and the differences between the Bragg rods arise strictly from the relative geometric arrangement of these hexagonal layers.

The reciprocal lattice positions with $h - k \neq 3n/7$ have negligible or zero intensities in the plane of water; these maxima occur at $K_z > 0$. This implies that the number of A, B and C type layers are the same. Moreover, these peaks are not at the same values of K_z. The symmetry between these peaks must be broken by allowing for lateral displacements between the layers. The effective geometrical structure factor can thus be written as

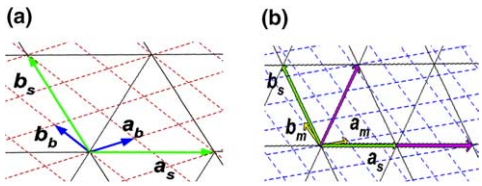

Fig. 4. Real space inorganic and organic lattices: (a) real space lattices of bulk hydrocerussite (---) (unit vectors $\underset{\sim}{a}_b, \underset{\sim}{b}_b$) and the $\sqrt{7}\times\sqrt{7}$ reconstructed surface (—) (unit vectors $\underset{\sim}{a}_s, \underset{\sim}{b}_s$); (b) real space lattice of the reconstructed surface (—) and the fatty-acid headgroups (---) (unit vectors $\underset{\sim}{a}_m, \underset{\sim}{b}_m$). The ratio of the unit cell areas is very close to 9.0. A close geometrical match is shown here, with the basis vectors for the two unit cells related by $2\underset{\sim}{a}_s = 5\underset{\sim}{a}_m - \underset{\sim}{b}_m$, $2\underset{\sim}{b}_s = \underset{\sim}{a}_m + 7\underset{\sim}{b}_m$.

$$F_{hk}(K_z) = \sum_{(h,k|h^2+k^2+hk=\text{constant}),j} 1 + \exp\left(\mathrm{i}\left(K_z C_j + 2\pi(hn_{1j} + kn_{2j}) + (h-k)\begin{pmatrix} 0 \\ -\frac{2\pi}{3} \\ \frac{2\pi}{3} \end{pmatrix}\right)\right)$$

where C_j represents the distance between the jth and the $j-1$th layer and n_{1j} and n_{2j} represent the lateral displacement along the two superlattice vectors in the jth layer. The last term represents the additional phase factor depending whether the layer is type A, B or C. There are 10 combinations of A, B and C type layers such that no layer is the same as adjacent layer. The best reproduction of peak positions and widths is obtained for ABCBCA type packing (Fig. 5(a)) with spacing between layers as 7.6, 8.1, 8.2, 8.9 and 9.2 Å and lateral displacements along the surface lattice vectors as $0.036\underset{\sim}{a}_s$, $-0.016\underset{\sim}{b}_s$ for the second and the third layers and $0.25\underset{\sim}{a}_s$ and $0.08\underset{\sim}{b}_s$ for the remaining three layers.

It is important to emphasize that our model is a simplified one and that other more complex and/or more realistic models can be proposed that will also fit the data. Our point is that the rod scans can be reasonably well fitted using a simple model with six atomic layers. The average interlayer spacing is consistent with the layer spacing for bulk hydrocerussite (8.2 Å).

Modification of the bulk hydrocerussite structure in a ~40 Å layer at the surface is the only plausible explanation for results described above. In studies of clean metal and semiconductor surfaces under UHV, similar surface superstructures have been identified, and attributed in various cases to rearrangement of surface bonds, coverage and arrangement of adsorbates, or vacancies and stacking faults in the surface layers [12–15]. In particular, $(\sqrt{7}\times\sqrt{7})$-$R19.1°$ surface reconstruction is quite familiar in UHV surface science [16,17].

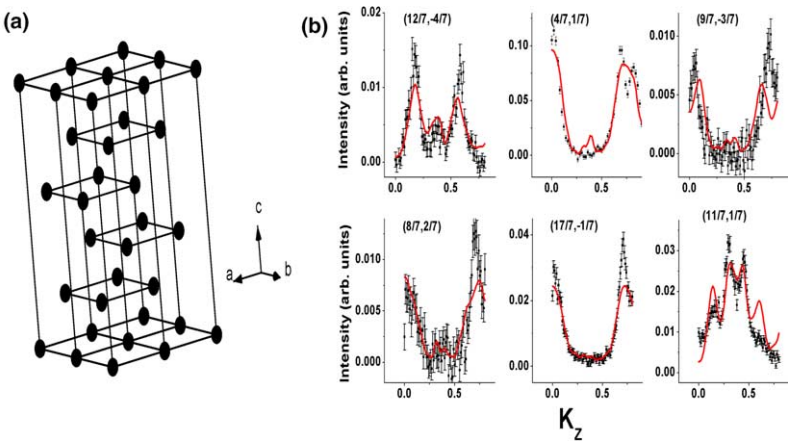

Fig. 5. Model for the reconstructed hydrocerussite layers that give a reasonable fit to our rod scan data: (a) real space representation of a $2\times2\times1$ cell of the ABCBCA type arrangement within the reconstructed layers; (b) Bragg rod scans of six surface lattice peaks. The solid curves are the results of simultaneous fits based on the six-layer model shown.

The structure of the organic monolayer template is also of interest. The ratio of the in-plane unit cell area of the surface structure to the area of organic lattice unit cell is very close to an integer (9.06). Organic lattices have been observed to adapt to adjacent surface structures [7]. This result suggests that the observed surface structure is at the upper surface of the hydrocerussite nucleate, between the organic monolayer and the bulk crystal. A close relationship between the organic and surface lattices consistent with an area ratio of 9 can be found (Fig. 4(b)), with a supercell twice that of the $\sqrt{7} \times \sqrt{7}$ lattice.

This is the first report of surface reconstruction under ambient conditions, without the use of UHV or high electrochemical potentials to keep surfaces clean. Our results show that bioinspired organic-template-directed growth can be just as precise a way of growing thin films as UHV methods are known to be. The reconstructed surface structure is stable during the full course of data accumulation (~6 h), indicating that the surface modification takes place in a relatively inert environment. Due to their acidic nature, fatty acid Langmuir monolayers do not interact strongly with aqueous anions, nor with monovalent aqueous cations below pH ~ 7 [18]. In addition, the existence of a lattice match may make the observed nucleation process energetically favored and thus selective, with impurities that might cause disorder or generate incommensurate structures being excluded from the interface. In other words, the organic–inorganic interface appears to be capable of providing a very clean and well-defined environment for the growth of inorganic films.

Acknowledgments

This work was supported by the U.S. Department of Energy under Grant No. DE-FG02-84ER45125. It was performed at beam line X14 of the National Synchrotron Light Source (NSLS) and at Sector I of the Advanced Photon Source (APS). We thank Dr. Peter Lee for his valuable assistance at APS and Dr. Jianming Bai for his help at NSLS.

References

[1] S. Mann, Biomineralization Principles and Concepts in Bioinorganic Materials Chemistry, Oxford University Press, Oxford, 2001.
[2] H. Rapaport, I. Kuzmenko, M. Berfeld, K. Kjaer, J. Als-Nielsen, R. Popovitz-Biro, I. Weissbuch, M. Lahav, L. Leiserowitz, J. Phys. Chem. B 104 (2000) 1399.
[3] V.M. Kaganer, H. Möhwald, P. Dutta, Rev. Mod. Phys. 71 (1999) 779.
[4] S. Mann, B.R. Heywood, S. Rajam, J.D. Birchall, Nature 334 (1988) 692.
[5] E.V. Rakova, V.V. Klechkovskaya, N.D. Stepina, L.A. Feigin, Cryst. Rep. 47 (2002) S177.
[6] B.R. Heywood, S. Mann, J. Amer. Chem. Soc. 114 (1992) 4681.
[7] J. Kmetko, C. Yu, G. Evmenenko, S. Kewalramani, P. Dutta, Phys. Rev. Lett. 89 (2002) 186102-1.
[8] J. Kmetko, C. Yu, G. Evmenenko, S. Kewalramani, P. Dutta, Phys. Rev. B 68 (2003) 085415-1.
[9] S. Barton, B. Thomas, E. Flom, S. Rice, B. Lin, J. Peng, J. Ketterson, P. Dutta, J. Chem. Phys. 89 (1988) 2257.
[10] V. Dupres, S. Cantin, F. Benhabib, F. Perrot, P. Fontaine, M. Goldman, J. Daillant, O. Konovalov, Langmuir 19 (2003) 10808.
[11] P. Martinetto, M. Anne, E. Dooryhée, P. Walter, G. Tsoucaris, Acta Cryst. C 58 (2002) i82.
[12] R. Feidenhans'l, Surf. Sci. Rep. 10 (1989) 105.
[13] I.K. Robinson, Phys. Rev. Lett. 50 (1983) 1145.
[14] D.K. Escott, S.J. Pratt, D.A. King, Surf. Sci. 562 (2004) 226.
[15] A.A. Stekolnikov, J. Furthmüller, F. Bechstedt, Phys. Rev. Lett. 93 (2004) 136104-1.
[16] P.A. Bennett, M. Copel, D. Cahill, J. Falta, R.M. Tromp, Phys. Rev. Lett. 69 (1992) 1224.
[17] S. Speller, T. Rauch, J. Bömmerman, P. Borrmann, W. Heiland, Surf. Sci. 441 (1999) 107.
[18] A. Datta, J. Kmetko, A.G. Richter, C.-J. Yu, K.-S. Chung, J.-M. Bai, P. Dutta, Langmuir 16 (2000) 1239.